Numerical-Probabilistic Assessment of Tempered Glass Failure based on the Generalised Local Model Characterised by Annealed Plates

A. Iglesias[a,b,*], M. Muniz-Calvente[c], A. Fernández-Canteli[c], I. Llavori[a], M. Martinez-Agirre[b], J. A. Esnaola[a]

[a] *Structural Mechanics and Design, Engineering Faculty, Mondragon Unibertsitatea, Arrasate-Mondragon, Spain*
[b] *Fluid Mechanics, Engineering Faculty, Mondragon Unibertsitatea, Arrasate-Mondragon, Spain*
[c] *Dep. of Construction and Manufacturing Engineering, University of Oviedo, Campus de Viesques, Gijón, Spain*

Abstract

Large-scale experimental programs become unavoidable to characterise the fracture behaviour of glass. Additionally, if non-uniform residual stresses are to be considered, the total effort required increases significantly. In this work, the primary failure cumulative distribution function (PFCDF) is derived from experimental annealed glass data. In this way, a novel methodology based on the characterisation of annealed glass to assess the failure of pre-stressed glass components is presented. Similarly, a joint evaluation of annealed and tempered glass is performed, thereby ensuring a higher reliability in the derivation of the PFCDF, which results in an average error below 10%.

Keywords: Generalised local model, fluid-structure interaction, probabilistic fracture design, annealed glass, tempered glass

Nomenclature

Greek letters

β	Shape parameter
δ	Scale parameter
δ_{eq}	Equivalent scale parameter
ε_{I}	Iterative relative difference
λ	Location parameter
σ	Residual stress [MPa]
$\sigma_{\max}$	Maximum principal stress [MPa]

Symbols

D	Jet diameter [m]

*Corresponding author at: Mondragon Unibertsitatea, Loramendi 4, Arrasate-Mondragon, 20500, Spain
Email address: aiglesias@mondragon.edu (A. Iglesias)

$F_{\max}$	Maximum experimental force [N]
GP	Generalised parameter
H	Jet-to-plate distance [m]
I	Iteration number
K	Stress intensity factor [MPa $m^{1/2}$]
P_{f}	Probability of failure
$P_{\mathrm{f,global}}$	Global probability of failure
P_{s}	Probability of survival
$P_{\mathrm{s,global}}$	Global probability of survival
S_{eq}	Equivalent size
S_{ref}	Reference size
T	Temperature [K]
t	Time [s]
t_0	Initial time [s]
t_∞	Steady-state time [s]
t_{cri}	Critical time [s]

Abbreviations

AA	Annealed glass
AT	Asymmetrically tempered glass
ATHD20	Asymmetrically tempered glass at short jet-to-plate distance
ATHD40	Asymmetrically tempered glass at large jet-to-plate distance
CDR	Coaxial double ring
CFD	Computational fluid dynamics
DIC	Digital image correlation
EFCDF	Experimental failure cumulative damage function
FEA	Finite element analysis
FEM	Finite element method
FSI	Fluid-structure interaction
GLM	Generalised local model
GP	Generalised parameter
HTC	Heat transfer coefficient
LEFM	Linear elastic fracture mechanics
PFCDF	Primary failure cumulative damage function

PIA	Principle of independent action
RS	Residual stress
SCALP	Scattered light polariscope
SIF	Stress intensity factor
ST	Symmetrically tempered glass
STHD20	Symmetrically tempered glass at short jet-to-plate distance
STHD40	Symmetrically tempered glass at large jet-to-plate distance
XFEM	Extended finite element method

1. Introduction

Over the last century, technological and engineering developments have modified the way people perceive glass, with a shift in perception from a fragile, aesthetic material to a structural material. Its theoretical tensile strength, which can be as much as 14 GPa, is thought to be sufficient for withstanding any external load [1]. Nevertheless, the surface damage produced during the manufacturing process, as well as subsequent handling, cutting, or usage, leads to the presence of microscopic flaws on the surface. Thus, in practical or everyday applications, ordinary glass does not exhibit pristine condition, and it might also be broken at loads as little as 7 MPa [2, 3]. The reason for this lies in the tendency of these microscopic flaws to propagate, particularly if the surface area is subjected to tensile loading.

Historically, glass was annealed in order to reduce or eliminate the tensile residual stresses developed during the manufacturing process [4]. Nevertheless, with the aim of developing compressive stresses on the surface and use glass as a structural material, the tempering process is most often applied. There are two existing types of tempering processes: chemical tempering and thermal tempering [2]. Both processes consist of developing superficial compressive stresses with the intention of strengthening glass [3, 5, 6]. However, as the chemical tempering implies a higher cost due to the specific equipment needed and a lower depth of layer, which refers to the thickness of the compressive stress layer in the material, thermal tempering becomes a more efficient method [7].

During thermal tempering, glass is heated to a uniform temperature at which it is fluid enough to relax internal stresses and rigid enough to avoid important deformations. Subsequently, different cooling techniques might be applied to chill the hot glass specimen. Air is the quintessential cooling technique employed to rapidly cool and strengthen the material due to its associated low cost [8, 9]. In this context, local flow phenomena during cooling play a far more vital role in the residual stress development of glass, as it results in non-uniform distributions [10, 11]. Additionally, several authors highlighted that more knowledge about the control of the heat treatment process was needed, as they observed high variations not only in the residual stress state of individual specimens but also among specimens of the same batch [12, 13]. Consequently, these inhomogeneities have a direct effect on the structural performance of glass.

By and large, the compressive stress layer originating in the heat treatment process may hamper crack propagation, but when components are subjected to large loadings, brittle materials are unable to redistribute these stresses, and catastrophic failure is bound to happen [8]. For this reason, prediction of the in-service behaviour of glass becomes paramount to preventing its structural collapse.

Historically, different approaches have been adopted to determine the influence of surface quality on the strength of glass. On the one hand, certain design guides or standards, such as the German technical guideline or the prEN 13474 standard, base their calculations on allowable stresses or safety factors due to its ease of implementation [14, 15, 16]. Nevertheless, the comparison between the calculated design strength and an allowable stress value might not result in accurate predictions, especially if safety applications are of concern. Moreover, the calculation of the strength of glass by European standards is controversial, as it is carried out differently among the various European member states [17]. On the other hand, the formulation based on linear elastic fracture mechanics (LEFM) is usually adopted for analysing the influence of defects on glass. In this context, Irwin identified the so-called stress intensity factor (SIF), K, to characterise material brittleness or fracture toughness [18, 19]. These developments gave rise to analytical formulations for investigating the influence of cracks. Lately, however, their application to complex problems has been outdated by numerical methods [20]. In this regard, a recent review summarised several numerical approaches for fracture simulations of laminated glass subjected to impact loading [21]. Among them is the element deletion method, which consists in removing the mass of the elements or setting the stress to zero to represent the failure of these elements. The use of cohesive zone models has also become popular. Cohesive zone models represent separation in the crack front based on phenomenological laws and have been found to be successful in analysing the impact failure behaviour of laminated glass and glass-PVB debonding [22]. Likewise, the calculation of SIFs based on the extended finite element method (XFEM) or the finite element method (FEM) has become common practice, particularly for modelling surface scratches [23, 24]. Nevertheless, these numerical methods become unfeasible if the whole population of microscopic flaws on the glass surface needs to be modelled. Thus, a probabilistic assessment of glass strength could be considered an appropriate method to account for the randomly distributed microcracks [25, 26, 27]. In this context, the Weibull distribution is reported to be the most widely used statistical approach for representing the fracture strength of brittle materials [28, 29]. While some works have performed direct statistical assessments of annealed and tempered glass panes, the results obtained are only representative of the specific geometry or load type analysed in the investigation [6, 30, 31]. Taking into account that large-scale experimental programs are essential for obtaining reliable cumulative distribution functions, this procedure might not be feasible if numerous features are to be investigated [32]. Furthermore, if non-uniform residual stresses are to be considered, the total effort required in the laboratory increases significantly. Thus, another common approach to assessing the strength of heat-treated glass implies the sum of the compressive pre-stress magnitude and the lower limit values of the statistical distribution of annealed glass. In this case, the 5% quantile of the distribution is usually considered. Nevertheless, Pisano et al. and Bonati et al. highlighted that the sum of the characteristic bending strength of annealed and heat-treated glass was not an appropriate approximation [29, 33]. They argued for the unlikelihood for both material strengths to simultaneously

attain their lower values at a given point. Consequently, this approach becomes too conservative, as the sum of both characteristic strengths is generally lower than the strength that is experimentally measured. Lately, phenomenological models have also gained traction. These models describe the fracture behaviour of the material based on empirical observations. As a result, they are not derived from fundamental theory and thus do not shed light upon the particular mechanisms involved in the fracture process. However, phenomenological models account for all the variables influencing the entire flaw population and become an accurate and cost-effective method for encompassing the statistical nature of glass. In this sense, Muniz-Calvente et al. proposed a generalised local model (GLM) establishing the concept of primary failure cumulative distribution function (PFCDF) [34]. As a result, complete transferability from the laboratory characterisation to the practical design of components was achieved. Moreover, different failure criteria based on the choice of the generalised parameter (GP) could also be taken into consideration. Consequently, the calculation of the PFCDF permitted to characterise the failure behaviour of a component, thereby ensuring the recognition of critial regions in parts subjected to specific loading conditions during the design process [35].

In summary, the strength of glass is heavily influenced by the presence of micro-cracks on the glass surface and the residual stress state. Owing to the existence of surface flaws, glass is prone to brittle fracture, and a probabilistic assessment becomes relevant to prevent its catastrophic failure. Similarly, a representative prediction of the residual stress pattern remains essential to analyse the in-service behaviour of the designed parts. It is, therefore, of great importance to develop a predictive model to determine the tempered state of glass and its in-service behaviour, reducing the huge experimental effort required when the fracture behaviour of pre-stressed glass components is analysed. Therefore, this paper presents a novel methodology based on the characterisation of annealed glass to assess the failure of pre-stressed glass components, considering both the non-uniform residual stress pattern and the statistical nature of glass strength. This approach is grounded on the fact that the amorphous structure of glass material remained unaltered, as the application of the heat treatment process or the residual stress development does not imply a phase transformation phenomenon. As a result, the intrinsic material remained unchanged, irrespective of the glass type employed. In this way, a cost-effective procedure to design the heat treatment process at an early stage of the production cycle, based on both the operational load distribution and the failure limit specified by the client, is provided.

The following section sets out the analysed case studies. Section 3 provides the theoretical formulation of the proposed numerical-probabilistic procedure. In Section 4, the experimental procedure is delineated. Section 5 is dedicated to a discussion of the results. Here, the numerical analysis and subsequent statistical assessments of the in-service behaviour of glass are validated against experimental data. Finally, the main conclusions of the investigation are presented.

2. Case studies

The samples used in this investigation were soda-lime square flat plates with a dimension of 90 x 90 x 4 mm. The edges of the plates were polished at the factory. Different glass types were investigated: annealed glass (AA),

symmetrically tempered glass (ST) and asymmetrically tempered glass (AT).

The as-received condition of the plates was annealed. Therefore, a tempering process was applied to develop residual stresses. For this purpose, specimens were symmetrically and asymmetrically tempered by two air nozzles. In addition, different jet-to-plate distances, H/D, were studied, where H is the distance to the plate and D is the nozzle diameter. To this end, a frame structure to hold the glass plates in a vertical position was designed and manufactured. To limit the thermal exchange between the glass sample and the supports, rock wool was used in the contact areas. Each contact area was limited to 5-10 mm on the edges of the plate. Figure 1 depicts the cooling unit for symmetrically and asymmetrically tempering glass plates.

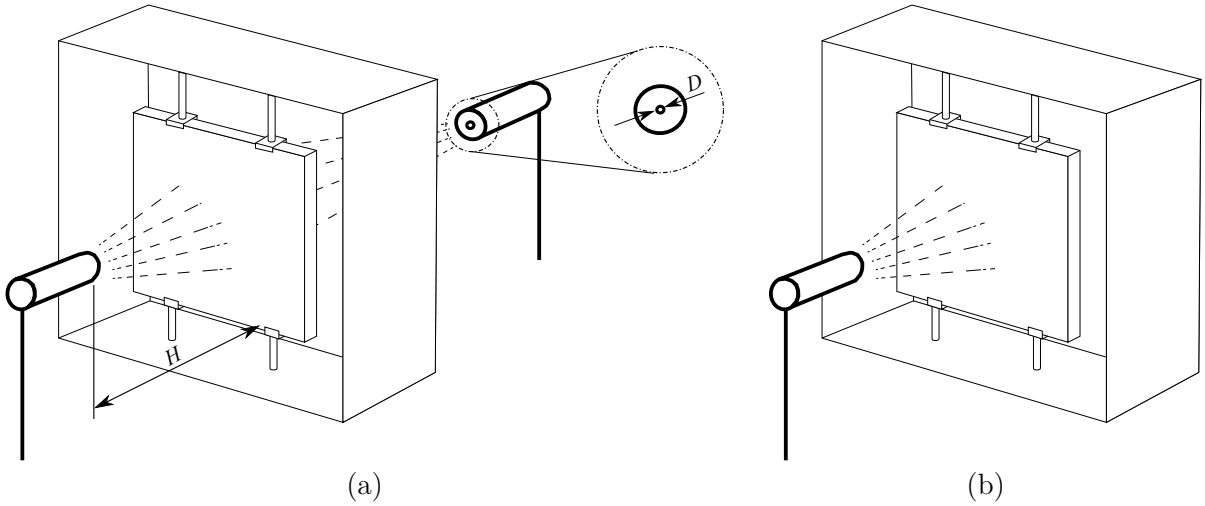

Figure 1: Cooling down unit of (a) symmetrically tempered glass plates and (b) asymmetrically tempered glass plates.

The symmetrical tempering tests were aimed to resemble the conventional residual stress pattern. Conversely, the asymmetric tempering configuration intended to offer a characteristic case of the tempering process, in which heat extraction by forced convection only occurred from one side of the plate. As a result, an asymmetric residual stress pattern was obtained. The standard tempering process tends to show slight asymmetric residual stress distributions due to the influence of rollers, even though differences tend to be small and residual stresses are often considered symmetrical [36]. Consequently, the asymmetric cooling configuration represents an extreme case, which results in an alternative stress state suitable to validate the proposed method.

A radiation furnace was preheated to 650 °C, and after holding each sample for 10 minutes, specimens were transferred to the tempering unit, where jets with an inlet diameter of $D = 3$ mm were used. Similarly, two jet-to-plate distances at $H/D = 20$ and $H/D = 40$ for each tempering configuration were selected. Higher H/D ratios than the standard tempering process were selected with a view to obtaining a more uniform stress distribution and preventing very localised and large residual stresses in the plate.

The brittle nature of glass makes the experimental strength characterisation a cumbersome process due to the exhibited large scatter of the results. With the aim of having a representative amount of samples according to UNE-

EN 1288-1 and UNE-EN 1288-5 standards, a total number of 30 samples were defined for each glass type [37, 38]. Table 1 summarises the analysed configurations as well as the corresponding number of samples.

Table 1: Overview of the proposed experimental program.

Glass type	H [mm]	H/D	Specimens
AA	-	-	30
ST	60	20	30
ST	120	40	30
AT	60	20	30
AT	120	40	30

Lastly, transversal loads are generally considered the main loads acting on structural glass plates. These loads may result from the effect of wind and snow on buildings and vehicles or assembly processes, such as installations of windows on their frame or car sunroofs. Nevertheless, an important factor to consider during the characterisation of glass strength is the crack orientation on the surface. however, there are numerous orientations, and the testing of an infinite number of samples becomes unfeasible. The use of coaxial double rings (CDR) enables one to assume an average probability of failure no matter the orientation of the prevailing crack. For this reason, the mechanical characterisation consisted of CDR tests at room temperature. For this purpose, the guidelines stated in the UNE-EN 1288-5 standard were followed [37]. An R30 ring configuration was used. The diameter of the load and support rings was 12 mm and 60 mm, respectively, and the curvature radius of both rings in the contact area was 2.5 mm.

3. Numerical-probabilistic procedure

The following numerical-probabilistic procedure is grounded in previous investigations carried out by the present authors in 2017 and 2022. Firstly, a one-way fluid-structure interaction (FSI) procedure for predicting the non-uniform residual stress distribution during tempering is used. Then, the GLM, which accounts for the local values in a component during loading situations, is adopted [34, 39]. The procedure consists of the following steps:

1. **Non-uniform residual stress prediction:** the 3D residual stress domain after the heat treatment process is predicted by a sequentially coupled FSI approach. Firstly, the commercial computational fluid dynamics (CFD) software Ansys Fluent is used to account for the local flow phenomena and to calculate the non-uniform temperature distribution on the plates. Then, the complete thermal history is read in the commercial finite element analysis (FEA) software, Abaqus FEA, to predict the non-uniform residual stress pattern of the component. Here, the material constitutive model considers the viscoelasticity and structural relaxation phenomena of glass based on the Narayanaswamy model [40, 41].

2. **Derivation of the PFCDF:** the final residual stress pattern developed in the heat treatment process is mapped into the structural FEM model. Similarly, an experimental program is carried out to characterise the failure of the

material. In this way, the local values of the reference or generalised parameter (GP) (e.g. maximum principal stress) in the specimen at the experimentally determined fracture loads are numerically calculated. The obtained local data is employed to derive the corresponding experimental failure cumulative damage function (EFCDF), and subsequently, the primary failure cumulative damage function (PFCDF) is calculated. The PFCDF is based on a three-parameter Weibull function, where the Weibull parameters are iteratively determined (see Equation 3). The derived PFCDF, identified as a three-parameter Weibull cumulative distribution function, permits the evaluation of the probability of failure, regardless of the specimen size, shape and load applied in the experimental characterisation. Consequently, it makes feasible the transferability of the results from the performed experimental work to the practical design.

Figure 2 presents the schematic overview of the proposed numerical-statistical procedure for predicting the probability of failure of structural glass components considering the non-uniform residual stress distribution.

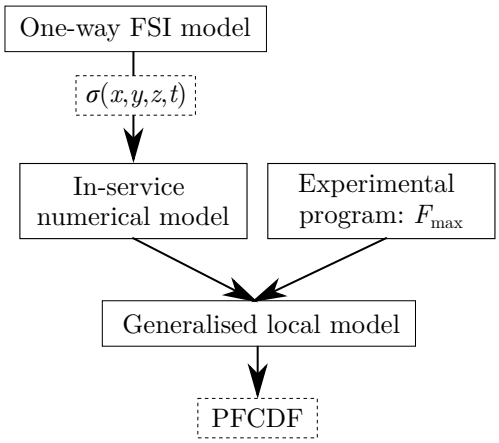

Figure 2: Flow chart of the proposed numerical-statistical procedure to predict the probability of failure of pre-stressed structural glass components.

Hereafter, the main aspects of the proposed method are outlined.

3.1. Proposed one-way FSI procedure

The numerical methodology based on a one-way FSI approach presented and validated by Iglesias et al. is proposed to capture the effect of non-uniform cooling on the residual stress distribution [39]. This procedure is based on two main assumptions: the low contribution of volumetric radiation to the thermal history of the material and the existence of a critical temperature. Thermal radiation in semi-transparent media gains special relevance as it becomes a bulk rather than a surface phenomenon. Nevertheless, thermal radiation also involves a high computational cost, as it depends on many parameters, such as direction, wavelength, time, the thickness of the material, boundary conditions and temperature distribution. However, when low-thickness glassware is tempered, the contribution of radiation to the temperature variation over time and to the final residual stress pattern becomes insignificant. Therefore, the

importance of volumetric radiation when low thickness glassware is subjected to large heat extractions, such as when air jet or mist cooling techniques are employed, was found to be low and, thus, was not considered within the model.

In addition to radiation phenomena, CFD simulations usually imply a high computational cost due to the involved physics, such as turbulence, heat transfer and the modelling of discrete particles. However, the structural relaxation of glass, which is known to be one of the main contributors to residual stresses, vanished around 400 °C [39]. Consequently, glass begins to behave as an elastic solid material, making the volumetric expansion lose traction. At this critical point, residual stresses are no longer influenced by cooling rate and become independent of thermal history. Therefore, a CFD model was defined with the aim of capturing the local flow phenomena during the initial stage of the cooling process. Once the critical temperature of 400 °C was reached, the initial thermal history was transferred to a thermal model where a constant and uniform heat transfer coefficient (HTC) was applied. Here, the remaining thermal history until room temperature was calculated. Finally, the complete thermal history was read into the structural model, and the non-uniform residual stresses were predicted. Figure 3 sets out the computational sequence of the proposed numerical procedure.

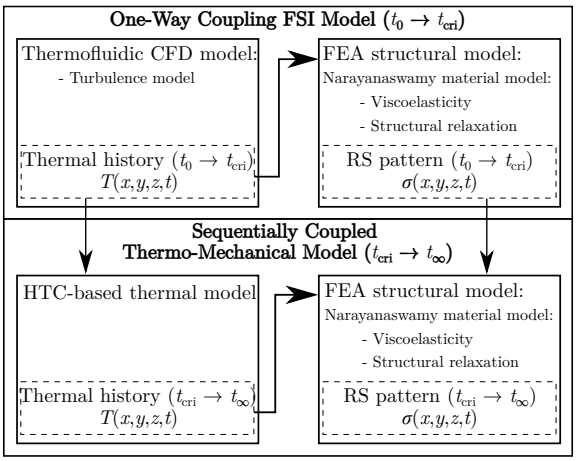

Figure 3: Flow chart of the proposed procedure to estimate the residual stress pattern over time, where a one-way FSI approach is proposed until the critical temperature instant (t_{cri}) is attained and a sequentially coupled thermo-mechanical approach is proposed from t_{cri} to steady-state temperature instant (t_∞). Reprinted from [39].

3.2. In-service numerical model

A numerical model based on the FEM was built to consider the local GP distribution on the glass surface. The model consisted of a load ring, support ring, silicon rubber and the glass specimen, as shown in Figure 4. The support ring was made out of steel and, hence, was considered a rigid body. The load ring was made out of aluminium and was considered deformable, as well as the silicon rubber and the glass plate. Table 2 sums up the material properties defined for each part based on the literature [42].

Two static general steps were defined. The first served as an approximation step until the load ring was put in contact with the sample, and the second acted as a loading step until the maximum experimental fracture load was

Table 2: General properties of glass, aluminium and silicon rubber at room temperature.

	Soda-lime glass	Aluminium 6000 series	Silicon rubber
Young Modulus [MPa]	70000	70000	20
Poisson coefficient	0.23	0.33	0.47
Density [kg/m^3]	2470	2700	950

attained.

With regard to the interaction between parts, a friction coefficient of 0.6 was assumed [43, 44]. The contact between the glass plate and the silicon rubber, as well as the rubber with the support ring, was described by a tie constraint. By this constraint, the selected surfaces were assumed to be bonded, and the stability of the numerical calculation was ensured.

As for the boundary conditions, the support ring was assumed to be fixed. Once the load ring interacted with the glass plate, a negative displacement based on the experimental tests in z direction was applied. Likewise, rotations were not hampered, but displacements in x and y directions in the central point of the glass plate were impeded until the loading step was initiated. Owing to the small size of the specimens, the bending action due to its own weight was neglected.

A total number of 54,077 elements were defined, from which 48,600 were associated with the glass specimen. Regarding the element type, quadratic full-integration hexahedral elements were selected. Six elements were defined through the plate thickness (Figure 4).

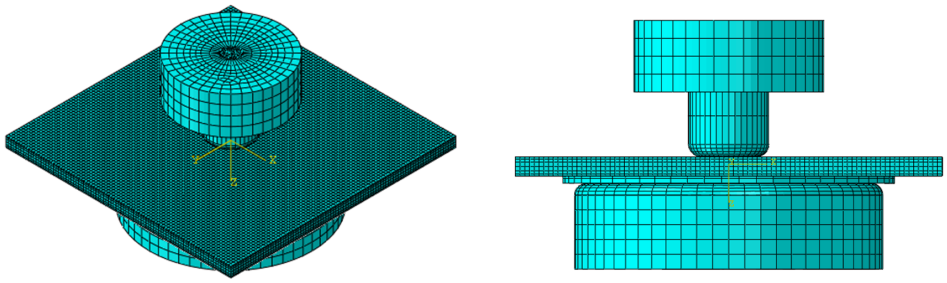

Figure 4: Mesh of the in-service model composed of a load ring, support ring, silicon rubber and glass specimen.

Finally, the final residual stress pattern obtained during the heat treatment calculation was mapped as an initial condition into the in-service model. In this way, residual stresses were taken into account and the local values of the generalised parameter (e.g. maximum principal stress) were obtained when the part was subjected to the maximum experimental forces.

3.3. Generalised local model

Here, the implemented statistical approach, which is based on the GLM proposed by Muniz-Calvente et al., is presented [34]. The aim of the GLM is to derive a PFCDF, which ensures the transferability from the laboratory characterisation to the design of components.

To this aim, the local stress distribution and the element size of the investigated glass conditions were numerically determined. Then, the numerical data was transferred to the GLM, where a reference size of 1 mm^2 was considered. The transferability of the results depends on the appropriate selection of the generalised parameter (GP) and the corresponding failure criterion to be applied in the failure prediction of the component. Based on experimental data, it is not obvious which stress criterion should be taken as a reference to derive the PFCDF. For this reason, two different criteria, namely, the maximum principal stress, $\sigma_{\max}$, and the principle of independent action (PIA) [45, 46], were considered as possible alternatives in the analysis.

$$GP = \sigma_{\mathrm{I}} = \sigma_{\max} \tag{1}$$

$$GP = (\sigma_{\mathrm{I}}^{m} + \sigma_{\mathrm{II}}^{m} + \sigma_{\mathrm{III}}^{m})^{(1/m)} \tag{2}$$

Based on the literature, a value of $m = 3$ is recommended for the PIA criterion [47]. The maximum principal stress criterion assumes that the material fails when the uniaxial tensile strength of the material is reached. Conversely, the PIA criterion is based on an equivalent stress that accounts for the principal stresses in the three principal directions. In this way, the biaxial stress state on the glass surface is taken into account. As the structural failure of glass commonly stems from the presence of tensile stresses, only the tensile mode of failure is considered, ignoring the influence of compressive stresses. Similarly, the failure mode of the material must be preserved. In this case, failure is assumed to occur due to the most unfavourable combination of defect size and stress level. As a result, the PFCDF for each glass type could be obtained.

The statistical assessment is divided into two stages. Firstly, the EFCDF for each glass sample is determined, from which, subsequently, the PFCDF is derived using the GLM. Secondly, a joint evaluation of the analysed glass types to increase the reliability of the predictions is also performed. Consequently, the formulation of both procedures is described hereinafter.

3.3.1. Single test assessment procedure

The GLM consists in an iterative process, which allows the failure model to be described as the three-parametric Weibull distribution, for a reference size S_{ref}, subjected to a uniform generalised parameter distribution. However, usual loading configurations show complex non-uniform distributions along parts. As a result, the three-parametric Weibull distribution to calculate the local probability of failure, $P_{\mathrm{f},S_{\mathrm{eq}}}$, is defined by the following expression:

$$P_{\mathrm{f},S_{\mathrm{eq}}} = 1 - \exp\left[-\frac{S_{\mathrm{eq}}}{S_{\mathrm{ref}}}\left(\frac{GP-\lambda}{\delta}\right)^{\beta}\right], \tag{3}$$

where λ is the location parameter, β is the shape parameter, and δ is the scale parameter. The model is defined by a generalised parameter, GP, which characterises the failure behaviour of the component when it acts uniformly on a reference size, S_{ref}. The equivalent size, S_{eq}, refers to the length, area or volume of a sample that, when subjected to the maximum value of GP, exhibits the same failure probability as the one obtained when the real component is subjected to the real GP distribution. In this context, Figure 5 shows the flowchart of the iterative process for fitting the three-parametric Weibull distribution.

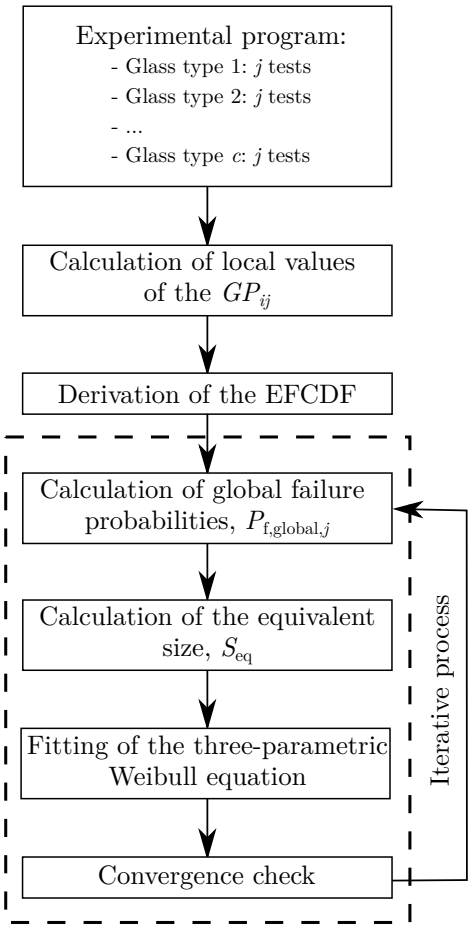

Figure 5: Flowchart of the calculation sequence to fit the three-parametric Weibull distribution.

Each step is briefly summarised in the following lines:

1. **Experimental program:** the first step consists in performing j experimental fracture tests for each of the c glass types under the same load conditions. Each glass type comprises $j = 30$ specimens with the same geometry but different residual stress patterns.

2. **Calculation of local values:** the load data obtained during the experimental fracture tests was used to numerically calculate the local distribution of the generalised parameter. Throughout this paper, the maximum principal stress or an equivalent stress in accordance with the PIA criterion was defined as the generalised parameter. As such, the GP_{ij} distribution on the component at the fracture instant was calculated where i refers to each element of the numerical model and j refers to the particular experimental test. Likewise, the element size of the defined grid was obtained.

3. **Experimental failure cumulative distribution function (EFCDF):** the EFCDF represents the relationship between the probability of failure and the critical value of the generalised parameter, namely, the value of GP_{ij} at the instant when each experimental sample collapses. The EFCDF depends on the test, applied load and the shape and size of the specimen. Its representation is given by a plotting position rule [48]. The critical values of GP_{ij} are sorted in increasing order, where a rank number and a probability of failure are associated with each test result. The failure probabilities are assigned using the following equation:

$$P_{\mathrm{f},j} = \frac{K_j - 0.3}{j + 0.4}, \tag{4}$$

where K_j ($K_j = 1...j$) refers to the rank order and j refers to the total number of tests per analysed glass type.

4. **Calculation of global probabilities of failure:** in this step, the global probability of failure is estimated by combining the local failure probabilities of all the elements of the component. The relationship between the local survival probability and the local failure probability is described by:

$$P_{\mathrm{s},S_{\mathrm{eq}},i} = 1 - P_{\mathrm{f},S_{\mathrm{eq}},i}. \tag{5}$$

Based on the weakest link theory, the global probability of survival refers to the multiplication of the survival probabilities of each link. Considering each link as a finite element, the global failure probability $P_{\mathrm{f,global},j}$ of each sample results from the combination of the probability of failure of each element:

$$P_{\mathrm{f,global},j} = 1 - \prod_{i=1}^{i_{\mathrm{total}}} (1 - P_{\mathrm{f},S_{\mathrm{eq},i}}) = 1 - \prod_{i=1}^{i_{\mathrm{total}}} \left(\exp\left[-\frac{S_{\mathrm{eq},i}}{S_{\mathrm{ref}}} \left(\frac{GP_{ij} - \lambda}{\delta} \right)^{\beta} \right] \right), \tag{6}$$

where $P_{\mathrm{f},S_{\mathrm{eq},i}}$ is the local probability of failure for the element i, $S_{\mathrm{eq},i}$ is the equivalent size of the element and GP_{ij} is the local value of the generalised parameter at the element i of each tested specimen.

5. **Calculation of the equivalent size:** the equivalent size of each specimen, $S_{\mathrm{eq},j}$, might be found by the following expression:

$$S_{\mathrm{eq},j} = -\log(1 - P_{\mathrm{f,global},j}) S_{\mathrm{ref}} \left(\frac{\delta}{GP_{\mathrm{max},j} - \lambda} \right)^{\beta}. \tag{7}$$

The global failure probability, the equivalent size and the Weibull parameters are initially unknown. With the view to starting the iterative process, some initial data is needed. Firstly, the initial values of λ, β and δ must be determined by fitting the EFCDF to a Weibull distribution function. Secondly, arbitrary values for the reference size and equivalent size were chosen. For the reference size, a similar size related to the analysed case is recommended, whereas, according to former experience, the equivalent size may be identified as 80% of the specimen or component size.

6. **Fitting the three-parametric Weibull distribution:** in this stage, the Weibull parameters are fitted. To this end, the Weibull parameters may be estimated by fitting the three-parameter Weibull cumulative distribution function to a straight line [49].

7. **Convergence criterion:** finally, the relative difference between the previous iteration (I - 1) with respect to the actual iteration I is calculated by:

$$\frac{|\lambda_I - \lambda_{I-1}|}{\lambda_I} + \frac{|\beta_I - \beta_{I-1}|}{\beta_I} + \frac{|\delta_I - \delta_{I-1}|}{\delta_I} < \varepsilon_{\mathrm{I}}. \tag{8}$$

When the iterative relative difference is below $\varepsilon_{\mathrm{I}} < 10^{-9}$ convergence is attained. If not, the iterative process continues and the actual values are transferred to the calculation of the global probability, thus updating the equivalent size calculation and the respective Weibull parameters.

3.3.2. Joint test assessment procedure

Based on the GLM, the joint evaluation enables all the experimental case studies to be considered a unique experimental program. As a result, the larger amount of experimental data employed leads to a more reliable prediction of the probability of fracture. The aim of this evaluation is to derive a master PFCDF as material property [47]. Figure 6 sets out the flowchart for fitting the three-parametric Weibull distribution based on all the performed experiments.

In the following lines, each step is delineated:

1. **Verification of the transferability of the results:** first, the failure criteria and the transferability between the analysed case studies must be checked.

2. **Calculation of the global probabilities of failure:** as the joint Weibull parameters in the first iteration are still unknown, the minimum value of λ and the mean values of β and δ of the PFCDFs to be derived and merged are taken into account. In this way, the global probability of failure for each test at the first iteration is calculated by the following expression:

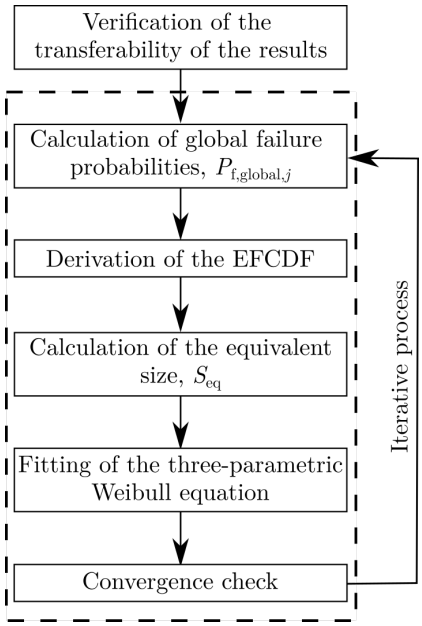

Figure 6: Flowchart of the calculation sequence to fit the three-parametric Weibull distribution by the joint test evaluation.

$$P_{f,global,j} = 1 - \prod \left(1 - P_{f,S_{eq,ij}}\right) = 1 - \prod \left(\exp\left[-\frac{S_{eq,ij}}{S_{ref}}\left(\frac{GP_{ij} - \lambda}{\delta}\right)^{\beta}\right]\right). \tag{9}$$

3. **Calculation of the EFCDF:** the maximum GP values of each glass type batch are ranked in ascending order, and a probability of failure is assigned to each of them using the aforementioned plotting position rule (see Equation 4).

4. **Calculation of new equivalent sizes:** an equivalent reference size must be assigned to each GP value to carry out the joint assessment. The following equation permits the calculation of the equivalent scale parameter, δ_{eq}, for each critical GP value of each sample, $GP_{max,j}$:

$$\delta_{eq,j} = \frac{GP_{max,j} - \lambda}{[-\log(1 - P_{f,global,j})]^{(1/\beta)}}. \tag{10}$$

The equivalent scale parameter enables the calculation of the equivalent size. In this way, the conversion of the cumulative damage functions to an equivalent-size specimen is performed using the following formulation:

$$S_{eq,j} = \frac{S_{ref}}{(\delta_{eq,j}/\delta)^{\beta}}. \tag{11}$$

As a result, the GP values of each experimental test are shifted and sorted, giving rise to a unique master curve.

5. **Fitting the three-parametric Weibull parameters:** once the equivalent size is calculated, the Weibull parameters

are fitted using a standard procedure [49].

6. **Convergence criterion:** if the relative difference is below the defined threshold (see Equation 8), the iterative process is brought to an end. If not, the iterative process continues, and the actual values are transferred to Step 2. As a result, the Weibull parameters of the joint PFCDF are obtained.

Finally, the experimental results might show large scattering due to the randomly distributed cracks on the surface. As a result, the calculation of confidence intervals becomes necessary to assess the reliability of the predictions. In fact, certain standards, such as UNE-EN 1288-1, encourage determining the confidence intervals to better represent the statistical uncertainty involved in these experiment programs [38]. With this in mind, these intervals were obtained by the bootstrap method and were also included in the subsequent analysis.

4. Experimental procedure

The experimental procedure consisted of two parts. Firstly, the heat treatment of the samples was carried out, and residual stress measurements were taken. Secondly, bending strength characterisation tests were carried out.

4.1. Glass tempering tests

As explained in Section 2, five different batches comprising different glass types were analysed, namely, annealed and tempered glass, the latter of which exhibited four different residual stress distributions, more specifically: annealed glass (AA), symmetrically tempered plates at $H/D = 20$ (STHD20) and $H/D = 40$ (STHD40) and asymmetrically tempered plates at $H/D = 20$ (ATHD20) and $H/D = 40$ (ATHD40). For this purpose, as-received glass samples needed to be tempered.

The tempering unit was composed of one DAG PRESTO GOLD nozzle on each side of the plates and connected by flexible air hoses. In the same manner, a flow meter was employed to control the pressure and flow rate, and an on/off switch was used to activate the air supply. A radiation furnace NABERTHERM LH60/14 was employed for the heat-treating the samples. Firstly, temperature control of the heating process was carried out with a National Instruments data acquisition system controlled by LabVIEW. A 4 slot NI cDAQ chassis with a 9213 module was used to record the data from the temperature sensors. To this end, three N-type thermocouples were attached to the glass surface with OMEGA CC high-temperature cement. Then, the furnace was preheated at 650 °C, and a heating cycle of 10 minutes was defined based on the thermocouple measurements. Once the furnace was heated up to 650 °C, glass samples were successively introduced into the furnace. After the defined heating period finished, the frame was transferred to the cooling unit.

At this stage, thermography-based temperature measurements were also taken with a FLIRT1030Sc thermographic camera. Likewise, the high emissivity ceramic coating AREMCO 840-CM, with an emissivity chart provided by the supplier, was used to paint the surface of the plate and record the temperature during cooling (see Figure 7).

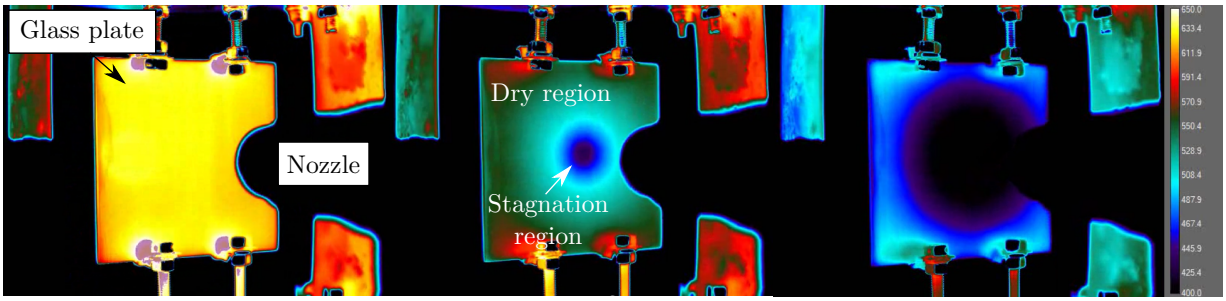

Figure 7: Temperature distribution on the glass surface recorded by thermography during the cooling down process.

Finally, non-destructive residual stress measurements by means of a portable scattered light polariscope (SCALP) were taken on five heat-treated samples to ensure the repeatability of the heat treatment process. The SCALP-05 developed by GlasStress Ltd. was used to measure the residual stress distribution in the quenched glass plates. This instrument can measure thickness residual stresses up to 6 mm. To determine the residual stress magnitudes and distribution on the surface, the SCALP, together with a CNC coordinate machine, was employed. This provided automated control in the x and y directions.

4.2. Coaxial double ring tests

The UNE-EN 1288-5 standard specifies the procedure and parameters to determine the bending strength of small glass samples by the use of coaxial rings [37]. Both rings were designed and manufactured in accordance with the specifications given in the UNE-EN 1288-5 standard. Similarly, an additional support manufactured by 3D printing was used to ensure the alignment of the samples with respect to the testing machine.

An MTS uniaxial testing machine with a 15 kN load cell was employed. Methacrylate panes were used to ensure the required safety conditions, and a self-adhesive film was employed on the not loaded surface, namely the side placed under compression during loading, as recommended in the UNE-EN 1288-5 standard. The aim of this film was to ensure that the origin of fracture occurred in the load ring area by analysing the post-fracture arrangement of the pieces on the tested glass specimen. In the same manner, a silicon rubber was located between the support ring and the sample to achieve a uniform reaction throughout the support area. In the case of asymmetrically tempered plates, the downward surface, which is subjected to tensile stresses during loading, is exposed to fracture and referred to as the air-impinged surface. A loading rate of 2 MPa/s was defined until the fracture of the specimen occurred. Finally, the vertical displacement field was also investigated by applying the digital image correlation (DIC) technique using the ARAMIS 3D equipment of the GOM company. Three samples (T1-T3) for each glass type were measured, and a mirror inclined at 45° was used to capture the downside view of the plates and record the displacement field during the tests (see Figure 8).

As a result, the variation of the displacement distribution of each sample during the loading period could be recorded. With the aim of validating the numerical results, an average experimental displacement contour was calculated based on the measured samples for each glass type. Then, the vertical displacement distribution along x and y

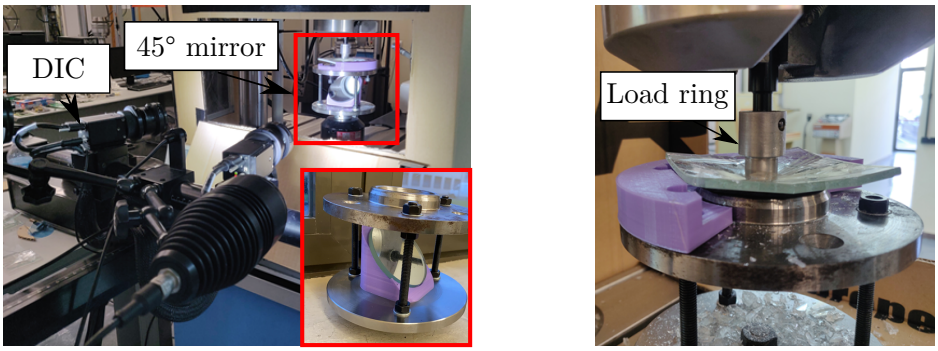

Figure 8: Experimental CDR set-up: (a) ARAMIS 3D GOM equipment with an inclined mirror at 45°, and (b) CDR test until fracture of the specimen.

directions were obtained. In this way, a scattering band could be built to compare the numerical calculations to the experimental measurements. Figure 9 illustrates the post-processing procedure to represent the CDR test results.

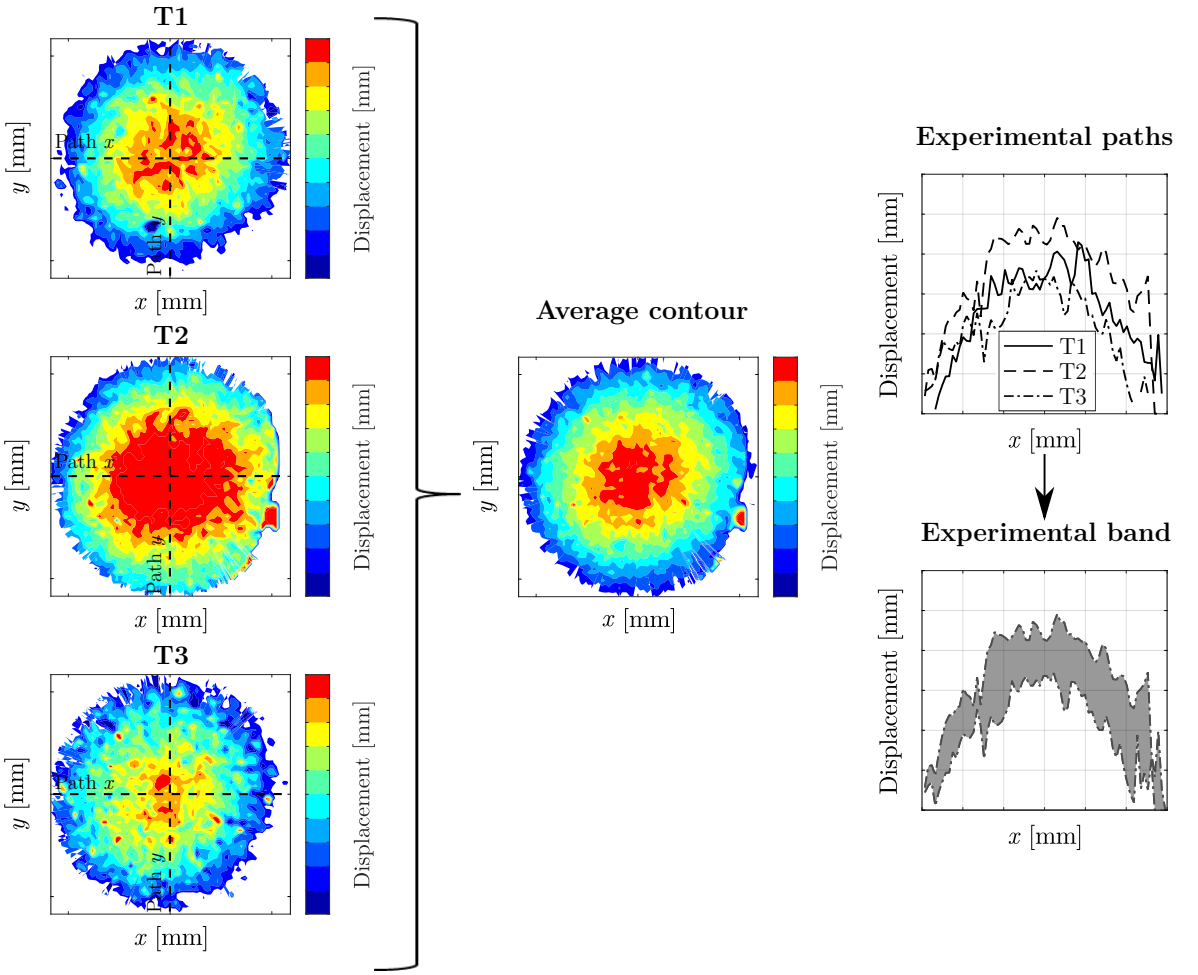

Figure 9: Experimental post-processing procedure for the results of the CDR tests.

5. Results and discussion

This section moves on to validate the proposed numerical-probabilistic procedure. Firstly, the residual stress predictions and the numerical model consisting of the coaxial double ring set-up are validated. Then, a single test statistical assessment to derive the PFCDF of each glass type is carried out. Two different failure criteria are considered as possible alternatives in the assessment. The failure probabilities of annealed and tempered glass are predicted not only based on their own experimental data but also based on experimental data from the remaining glass types. In this way, the most suitable failure criterion is selected, and the transferability of the results is verified. Finally, a joint assessment of the analysed glass types is performed by merging the data of each glass type as a unique experimental program.

5.1. Residual stress calculation

Prior to validating the modelling of the fracture characterisation, the residual stress distribution of each analysed tempering configuration was compared to experimental data. For annealed glass, a stress-free plate was assumed. Hence, in this section, the validation of the numerically predicted stress pattern on the downward surface, namely, the surface subjected to tensile stresses during the CDR tests of symmetrically and asymmetrically tempered glass plates is presented.

Figure 10 illustrates the contour plots of residual stress distributions for symmetrical tempering plates at H/D = 20: (a) average experimental measurement, (b) numerical prediction and (c) the relative difference. To this end, two different regions were distinguished on the surface of the plate (see Figure 7). On the one hand, the stagnation or jet facing area refers to the zone where the jet flow collided with the targeted surface. On the other hand, the dry region refers to the area towards the edges of the plate where the influence of the impingement flow lost traction, and hence, heat extraction became lower. Local differences with respect to the average experimental contour of up to 5% and 20% in the stagnation and dry regions were observed, respectively.

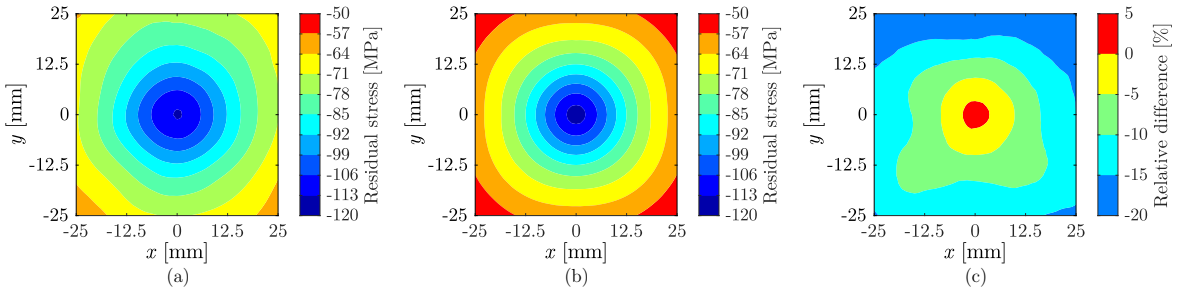

Figure 10: Residual stress distribution on the front surface of symmetrically tempered glass samples at H/D = 20: (a) experimental average, (b) modified procedure, and (c) deviation.

Figure 11 shows the average experimental residual stress, the numerical residual stress and the deviation distributions for symmetrical tempering plates at H/D = 40. In this case, a homogeneous average deviation of around 12% was observed.

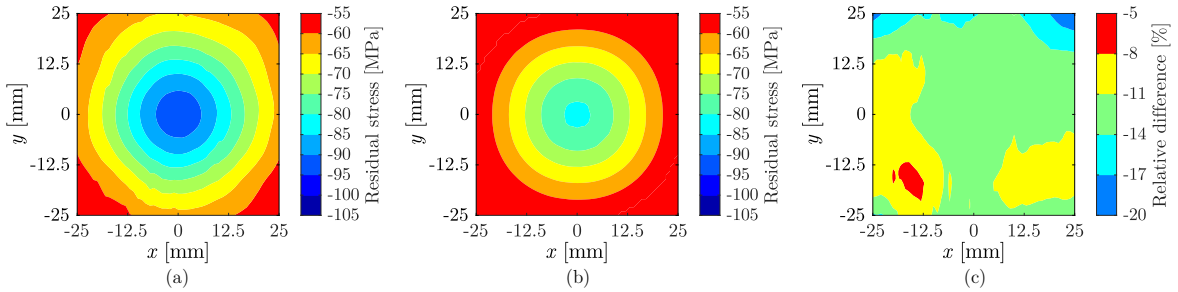

Figure 11: Residual stress distribution on the front surface of symmetrically tempered glass samples at $H/D = 40$: (a) experimental average, (b) modified procedure, and (c) deviation.

Likewise, Figure 12 depicts the contour plots of the average experimental and numerical residual stresses and the relative difference distribution for asymmetrical tempering plates at $H/D = 20$. Differences in the residual stress distribution up to 10% and 20% were perceived in the stagnation and dry regions, respectively.

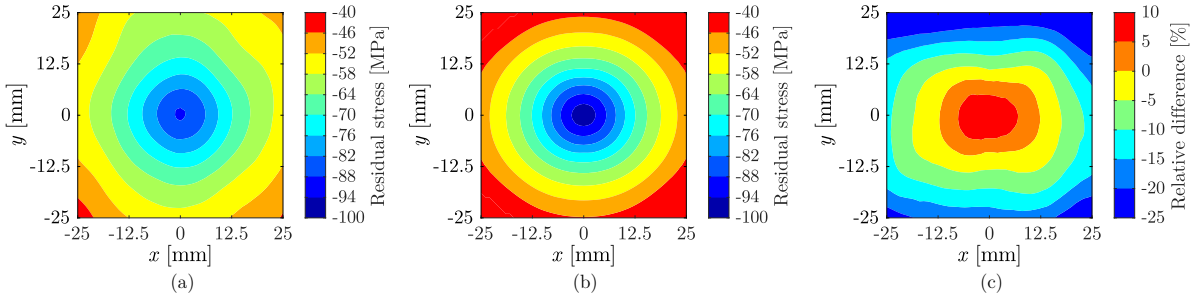

Figure 12: Residual stress distribution on the front surface of asymmetrically tempered glass samples at $H/D = 20$: (a) experimental average, (b) modified procedure and (c) deviation.

Figure 13 presents the average experimental residual stress and the estimated residual stress distributions, as well as the deviation among them for asymmetrical tempering plates at $H/D = 40$. Similar conclusions could be drawn in this case, as differences ranged from 5% to 25% on the surface.

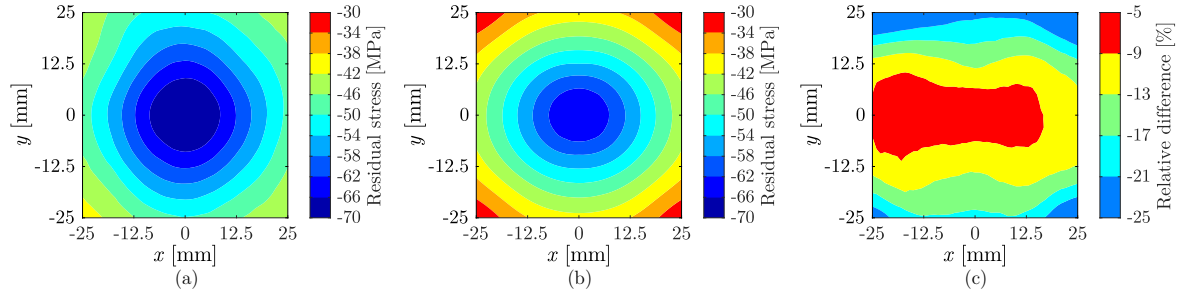

Figure 13: Residual stress distribution on the front surface of asymmetrically tempered glass samples at $H/D = 40$: (a) experimental average, (b) modified procedure and (c) deviation.

In addition to the residual stress distribution, residual stress paths crossing at the centre of the plates were also investigated. Here, the numerical estimation with respect to the measured experimental band and the uncertainty

range of 5% of SCALP was provided. As a result, Figure 14 plots the calculated stress distributions along the x and y directions for symmetrically tempered plates at $H/D = 20$.

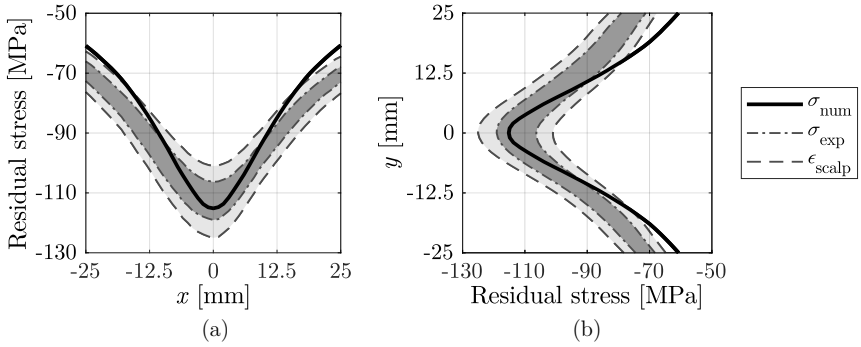

Figure 14: Residual stress distribution on symmetrically tempered glass samples at $H/D = 20$ along (a) x direction and (b) y direction.

The predicted residual stress distributions were found to be in agreement with the experimental measurements, as broadly fell within the specified bands. Larger differences were perceived in the dry regions of the plate, namely in the regions where less heat extraction occurred. The reason for this may be related to experimental uncertainties, such as the quench delay, which affects the initial quenching temperature. The quench delay refers to the time period from the opening of the furnace door to the cooling initiation. As a result, dissimilar initial temperatures can be obtained, which was found to have a significant impact on residual stress distributions [39]. Figure 15 presents the estimated residual stress distribution along x and y directions for symmetrically tempered plates at $H/D = 40$.

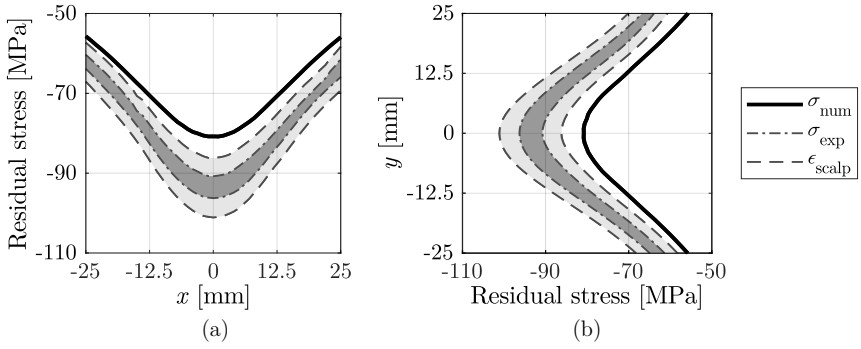

Figure 15: Residual stress distribution on symmetrically tempered glass samples at $H/D = 40$ along (a) x direction and (b) y direction.

In this case, the predicted residual stress distributions remained in the lower limit of the specified experimental bands. In part, these differences could be explained by possible uncertainties regarding the modelling of turbulent flow at large jet-to-plate distances. Turning to the asymmetric tempering results, Figure 16 sets out residual stress paths along the x and y directions of the plates asymmetrically tempered at $H/D = 20$.

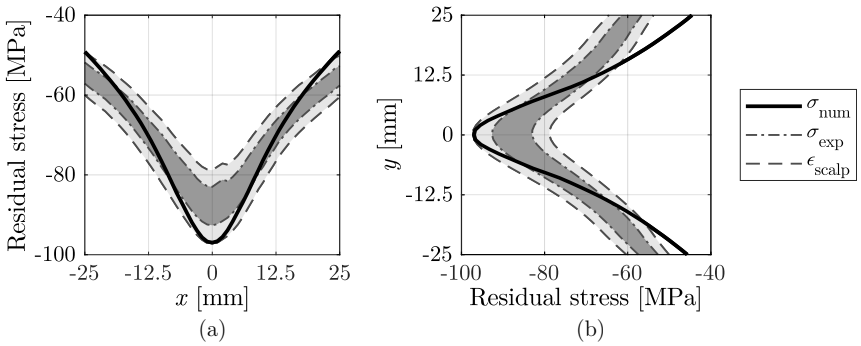

Figure 16: Residual stress distribution on asymmetrically tempered glass samples for H/D = 20 along (a) x direction and (b) y direction

The estimated residual stress distributions were considered representative, as most remained within the specified experimental bands. Deviations were particularly observed towards the dry regions of the plate, where forced convection lost traction. These facts came along with the estimated residual stress distribution along the x and y directions of samples asymmetrically tempered at H/D = 40, as depicted in Figure 17.

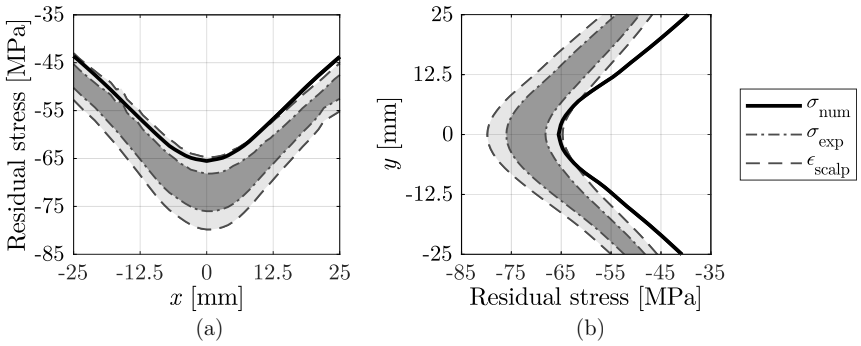

Figure 17: Residual stress distribution on asymmetrically tempered glass samples for H/D = 40 along (a) x direction and (b) y direction

As the jet-to-plate distance increased, forced convection became less significant. The calculated residual stress distributions on the load application area were within the measured experimental bands. As a result of all the above, the predicted residual stresses were considered representative for this analysis.

Table 3: Experimental fracture loads for each glass type: annealed (AA), symmetrically tempered glass at $H/D = 20$ (STHD20) and $H/D = 40$ (STHD40) and asymmetrically tempered glass at $H/D = 20$ (ATHD20) and $H/D = 40$ (ATHD40).

Fracture loads, F_{max} [N]				
AA	STHD20	STHD40	ATHD20	ATHD40
827	2498	2210	2020	1941
948	2632	2370	2081	2056
956	2865	2436	2191	2096
969	2869	2542	2253	2113
1026	2903	2562	2280	2160
1052	2928	2675	2389	2220
1096	2975	2737	2406	2237
1103	2977	2749	2430	2239
1136	3017	2846	2497	2250
1154	3034	2862	2502	2278
1161	3050	2882	2514	2322
1177	3070	2889	2521	2335
1254	3162	2914	2582	2350
1298	3188	2917	2626	2350
1309	3198	2969	2702	2366
1317	3228	2973	2717	2387
1436	3232	2977	2743	2394
1580	3258	2980	2756	2398
1678	3302	3067	2756	2439
1714	3309	3108	2761	2472
1793	3315	3112	2790	2475
1803	3340	3247	2822	2486
1945	3351	3281	2877	2499
2005	3441	3288	2888	2526
2053	3480	3305	3002	2707
2103	3511	3425	3031	2753
2257	3618	3493	3057	2828
2282	3667	3964	3088	2834
2319	3679	4021	3269	2834
2712	3729	4854	3412	3146

5.2. Bending strength calculation

Once the predicted residual stresses were validated, the maximum displacement attained during the fracture characterisation was studied. Table 3 shows the fracture loads obtained during the CDR tests for each glass type.

To validate the calculation of the local stress distributions at each fracture load, the numerical maximum displacement field and the displacement distributions measured by DIC at different time frames were investigated. As three samples were recorded for each glass type, an average experimental displacement distribution was calculated as shown in Figure 9, and vertical displacement paths along x and y directions crossing at the centre of the plate were defined. Figure 18 sets out the displacement magnitude in both directions for annealed glass at 500 N and 1000 N.

Figure 19 shows the displacement along the defined paths for symmetrically tempered glass ($H/D = 20$) at 1000,

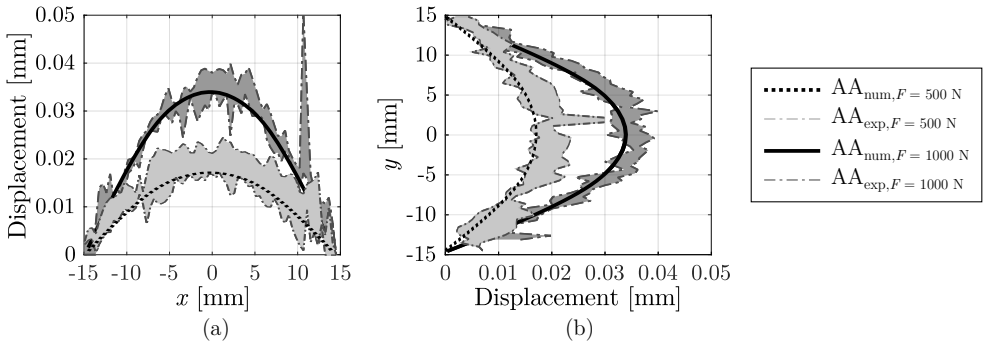

Figure 18: Comparison between experimental and numerical displacement paths in annealed glass specimens along (a) x direction and (b) y direction.

2000 and 3000 N.

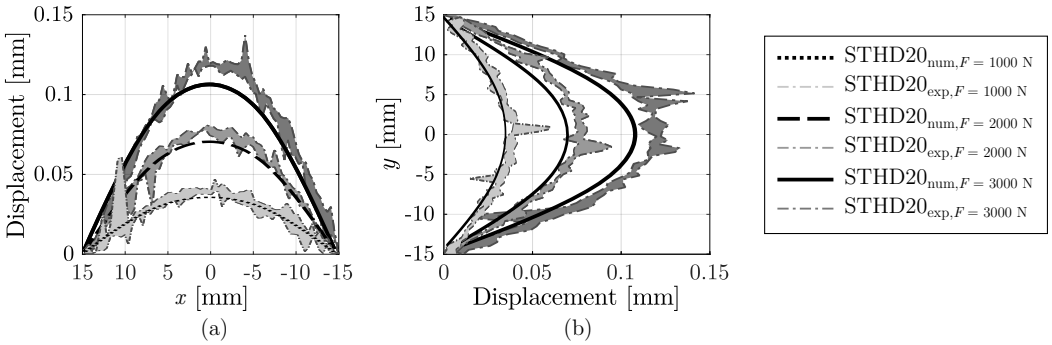

Figure 19: Comparison between experimental and numerical displacement paths of symmetrically tempered glass samples for H/D = 20 along (a) x direction and (b) y direction.

Figure 20 shows the vertical displacement value along the x and y directions for symmetrically tempered glass (H/D = 40) at 1000, 2000 and 3000 N.

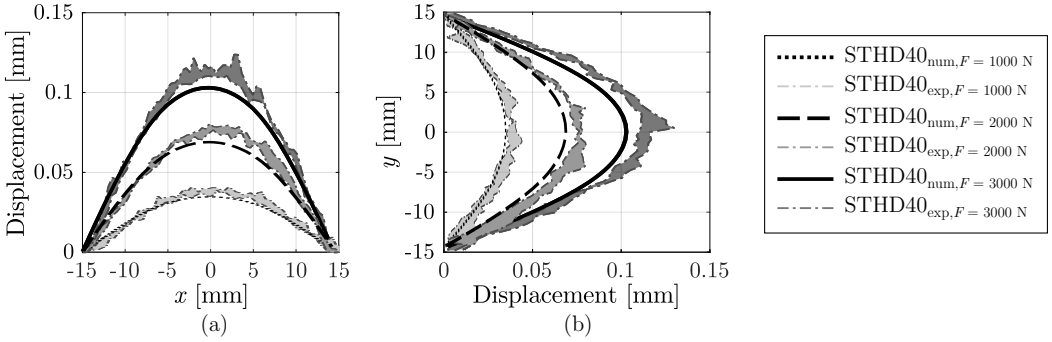

Figure 20: Comparison between experimental and numerical displacement paths on symmetrically tempered glass samples for H/D = 40 along (a) x direction and (b) y direction.

Figure 21 sets out the displacement along the defined paths for asymmetrically tempered glass (H/D = 20) at 1500

and 2500 N.

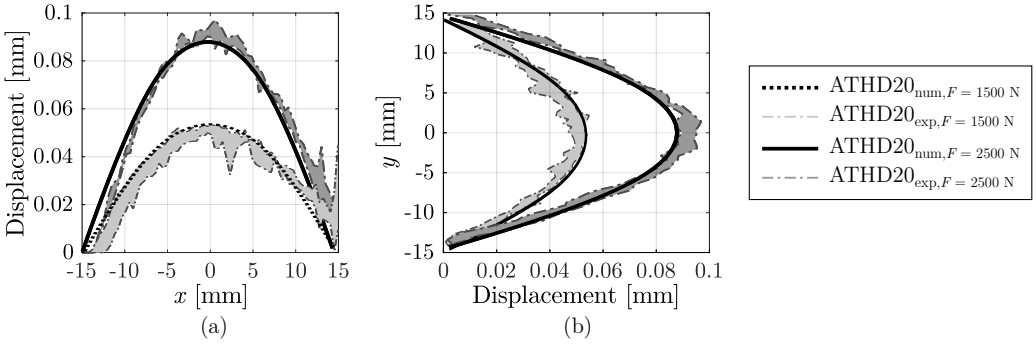

Figure 21: Comparison between experimental and numerical displacement paths on asymmetrically tempered glass samples for $H/D = 20$ along (a) x and (b) y directions.

Finally, Figure 22 shows the vertical displacement value along the x and y directions for asymmetrically tempered glass ($H/D = 40$) at 1500 and 2500 N.

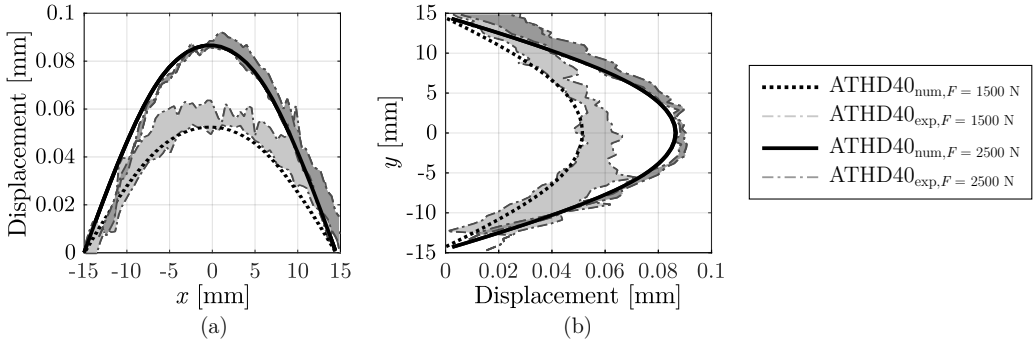

Figure 22: Comparison between experimental and numerical displacement paths on asymmetrically tempered glass samples for $H/D = 40$ along (a) x and (b) y directions.

In summary, the relative error of the numerical model with respect to the experimental results remained below 10% in all the analysed cases.

5.3. Single test statistical assessment

In this section, a statistical assessment of the fracture characterisation of glass is performed. Firstly, the local stress distributions of the investigated glass types were numerically determined. Then, the numerical data was transferred to the GLM. Regarding the failure criteria, based on the obtained experimental data, it is not obvious which stress or stress combination should be taken as a suitable reference to derive the PFCDF. For this reason, two alternative criteria, namely, the maximum principal stress ($\sigma_{\max}$) and the principle of independent action (PIA), were analysed (see Equation 1 and Equation 2). Table 4 summarises the Weibull parameters for the considered glass type and failure criteria.

Table 4: Weibull parameters for each analysed glass type based on the maximum principal stress and PIA criteria.

Glass type	PIA			$\sigma_{\max}$		
	β	λ	δ	β	λ	δ
AA	2	42.92	2.28	2	35.17	2.07
STHD20	3.38	42.1	10.7	3.45	33.93	9.99
STHD40	2	66	2.35	2	53.74	2.16
ATHD20	3.01	23.7	9.11	3.05	20.85	8.42
ATHD40	2.16	69	1.76	2.05	57	1.33

Even if differences are perceptible among the calculated Weibull parameters, a good correlation between the analysed cases is proved in the following lines. This seems reasonable, as the artificial introduction of compressive stresses on the surface of specimens should not cause any alteration of the material structure. Moreover, with the aim of ensuring the transferability of the results among the investigated glass types, the derivation of the PFCDFs was not only based on the own experimental results of each glass type but also on the results of the remaining glass types. In this sense, Figure 23 sets out the predicted failure probability of annealed glass with the corresponding confidence intervals of 5% and 95%.

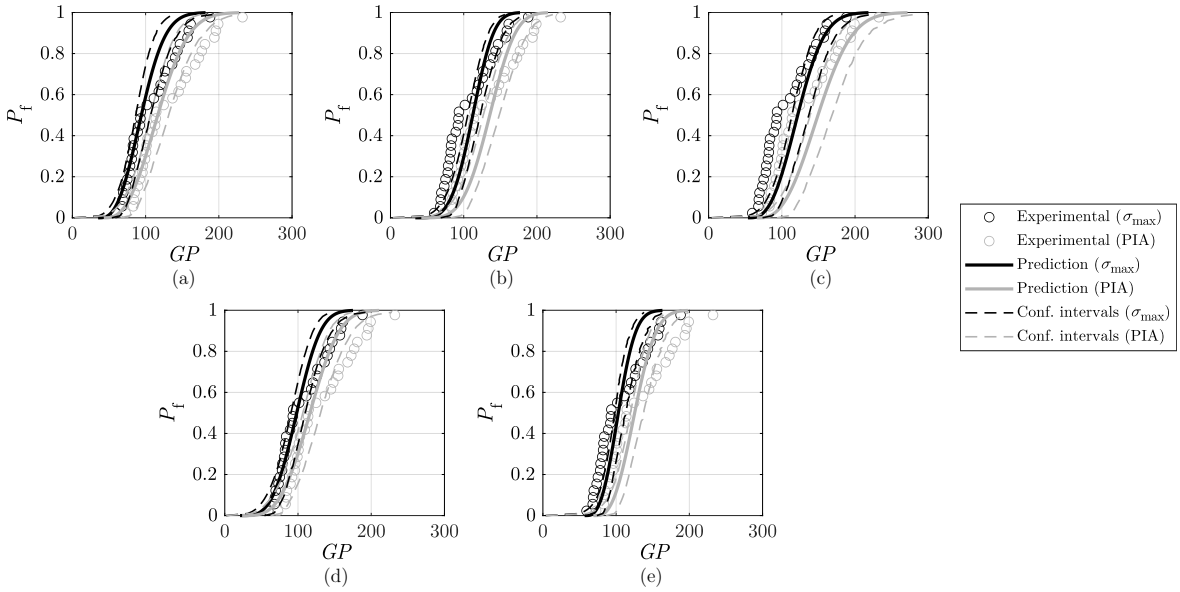

Figure 23: Failure probability prediction of annealed glass plates considering the PFCDF based on maximum principal stress and PIA failure criteria and derived from (a) own experiments, (b) STHD20, (c) STHD40, (d) ATHD20 and (e) ATHD40.

The predictions were based on the Weibull parameters derived from its own experimental data, in this case, annealed glass, and the remaining glass types (i.e., heat-treated glass). The predictions were observed to be in good agreement with the annealed glass experimental data. Based on its own experimental data, namely annealed glass data, short distance symmetric tempering (STHD20), and asymmetric tempering (AT) data, the relative average error of the predictions remained below 10%. The average deviation increased up to 15% for the large distance symmetric

tempering case (STHD40). Nonetheless, even if the stress results of specific regions were found to not be within the reliability intervals, in general, the calculated intervals tended to envelop the experimental measurements. The reason for this may be the limited number of experimental tests carried out. Nevertheless, the predictions based on different glass types were observed to behave in a representative manner. Likewise, both failure criteria showed appropriate representativeness of the experimental results, being the criterion of maximum principal stress the one exhibiting lower deviations. Nevertheless, these differences between both failure criteria were considered not significant, as they remained below 1%.

In this way, the transferability between the cumulative damage functions of annealed and tempered glass was ensured. Finally, Figure 24 shows the predictions made for tempered glass specimens based on the PFCDF derived from annealed glass experimental data.

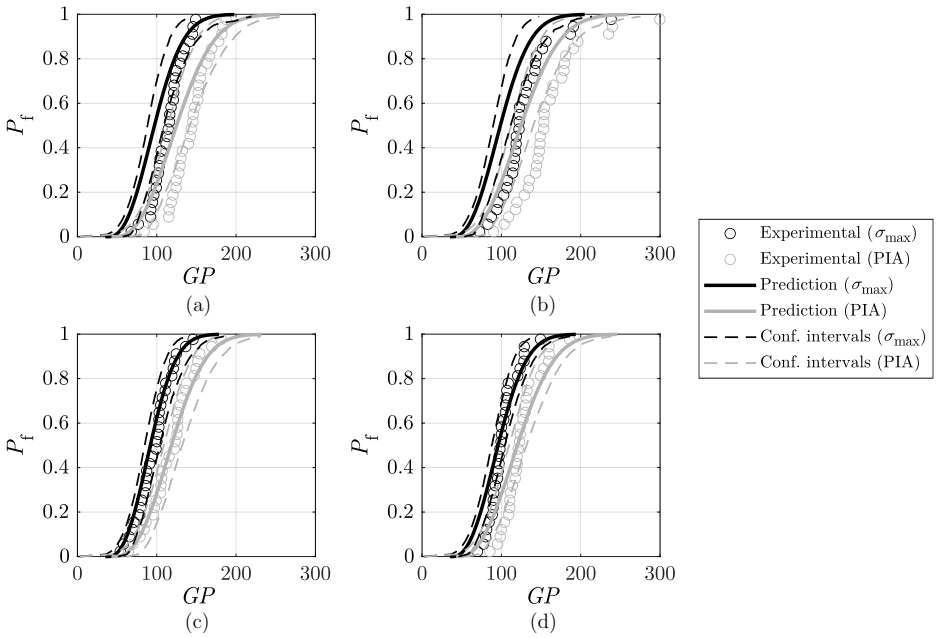

Figure 24: Failure probability of tempered glass plates considering the PFCDF based on maximum principal stress and PIA failure criteria and derived from annealed glass experimental data: (a) STHD20, (b) STHD40, (c) ATHD20 and (d) ATHD40.

What is striking about the data in Figure 24 is that the failure characterisation of annealed glass components could enable the estimation of the probability of failure of heat-treated glass. As a result, the derived PFCDF is not dependent on the glass type, namely, annealed or tempered, and the applied heat treatment. This result may be explained by the fact that the structure of glass is amorphous, and hence, the heat treatment did not signify a phase transformation in the material. Similarly, the surface condition of the annealed glass was verified to be similar to that before tempering. This meant that no surface treatments, such as artificial ageing of glass by sand abrasion, were applied before tempering. Consequently, the large experimental work needed for characterising the failure of structural glass components could be simplified due to the versatility that the derived PFCDF exhibited.

In summary, predictions were found to be in agreement with experimental data and broadly fell within the confidence intervals. Both failure criteria were considered to be representative, as the predictability of the probability of failure was found to be analogous. Slightly lower differences were observed for the maximum principal stress criterion, even if it does not account for the biaxial stress state arising in the CDR test. As the maximum principal stress criterion also involves an easier implementation than the PIA, this failure criterion was adopted for the subsequent analysis. This would be an interesting area for further work. Finally, the transferability of the results from one glass type to another was verified. For this reason, the next section moves on to perform a joint assessment to derive the generalised Weibull parameters that enabled the calculation of a master PFCDF.

5.4. Joint test statistical assessment

Once the transferability from one glass type to another was confirmed, the joint statistical evaluation of the experimental results was carried out. The aim of this analysis is to obtain a master PFCDF derived by merging all the data from the different experimental programs, which provides a higher level of reliability than that resulting from the individual experimental programs. For this purpose, the experimental data from the following glass types was merged: AA, STHD20, STHD40, ATHD20 and ATHD40.

Table 5 presents the Weibull parameters for the joint assessment based on the maximum principal stress criterion.

Table 5: Estimated Weibull parameters of the master PFCDF based on statistical joint assessment considering the maximum principal stress criterion.

	β	λ	δ
$\sigma_{\max}$	2.04	41.72	2.33

In this context, Figure 25 sets out the comparisons between the predictions and the experimental data of each analysed glass type based on the joining of all the experimental batches.

As observed, the derived master PFCDF permitted a reliable representation of the probability of failure of all the investigated glass types. In this case, the predicted failure probabilities showed an average error of up to 10% with respect to experimental measurements. Additionally, experimental data broadly fell within the confidence intervals, meaning that reliable predictions were obtained. Thus, the derived PFCDF was considered appropriate to predict the fracture behaviour of annealed and tempered glass.

Taken together, the derived master PFCDF permitted a more reliable representation of the probability of failure of the investigated glass types due to the larger amount of data points that, in addition, came from different batches. Additionally, the average relative difference remained at about 10%. Consequently, the versatility of the procedure for predicting the fracture behaviour of annealed and tempered glass was verified.

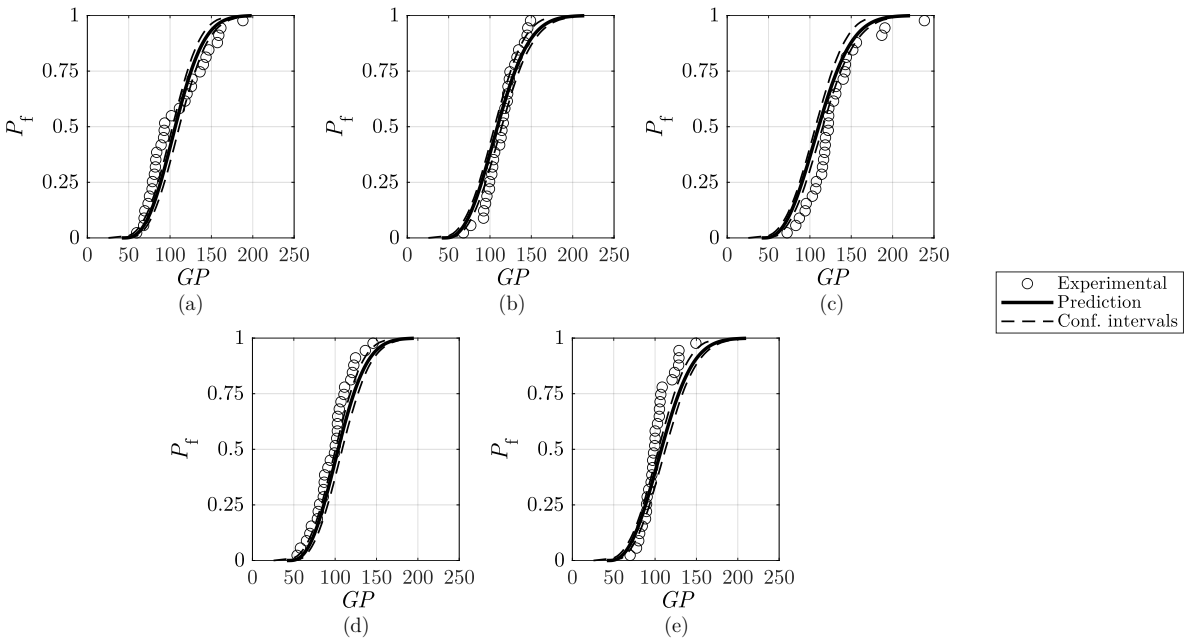

Figure 25: Joint evaluation based on the merging of all the experimental tests to predict the failure probability of (a) AA, (b) STHD20, (c) STHD40, (d) ATHD20 and (e) ATHD40.

6. Conclusions

A methodology to predict the failure of pre-stressed glass components based on the characterisation of annealed glass is presented and validated in this investigation. The main conclusions are set out below:

- A statistical-numerical model to evaluate the fracture probability of tempered glass components based on the fracture characterisation of annealed glass specimens was presented. The model accounts for any non-uniform residual stress distribution that may arise during the manufacturing or heat treatment process of glass. Therefore, the proposed numerical-statistical procedure becomes an efficient 3D method for predicting the failure probability of glass components, being independent of the inherent residual stress spatial distribution.

- The transferability between the failure cumulative functions of annealed and tempered glass exhibiting different residual stress patterns was confirmed. As a result, a PFCDF independent of the experimental specimen shape, size and applied load type was derived by means of the GLM. Therefore, the failure characterisation of annealed or tempered glass plates was proved to be valid in assessing the fracture design of either glass type. This means that for the analysed case studies, the failure criterion and the methodology to assess the global probability remain applicable irrespective of the initial residual stress distribution. Consequently, the need for resource-heavy large-scale experimental programs is reduced, which was previously the main drawback of assessing the in-service behaviour of pre-stressed glass.

- Once the transferability from one glass type to another was confirmed, all the experimental tests were merged

and jointly evaluated as a master PFCDF. The joint assessment facilitated a more reliable prediction of the fracture behaviour of both annealed and tempered glass. Overall, average relative differences between the predicted and experimental data were below 10%. Thus, the versatility of the procedure was verified. As such, the insights gained from this study can contribute to the development of a data-base, which becomes more reliable as the stored data grows.

- Regarding failure criteria, two alternative approaches were adopted, namely, the maximum principal stress and the PIA criteria. Both showed analogous predictive behaviour for the analysed case studies, with differences between them below 2%. The maximum principal stress criterion was therefore selected due to its easier implementation. Nonetheless, further investigation is recommended to attain a more in-depth knowledge of the influence of the failure criterion selection when considering residual stresses.

- Of particular note was the scatter band of the experimental results. Fracture strength data ranged from 50 and 250 MPa, resulting in a scatter of 200 MPa. Thus, an enhancement of the model could be expected if the number of tested samples was increased. This great variation in glass strength would suggest that statistical evaluation should be a mandatory step in the design and assessment of pre-stressed structural components.

- Finally, the natural progression of this work would be to extend the analysis to a real structural glass component. Thus, further investigation and application in an industrial case study is strongly recommended. Notwithstanding, this model sets the basis to make possible the ad hoc design of heat treatment processes early in the production cycle based on both the operational load distribution and the required failure probability specified by the client.

7. Acknowledgments

The authors would like to acknowledge the financial support provided by the Basque Government by means of Research Groups (IT1505-22 and IT1316). The authors want also to acknowledge the help provided by Miguel Lozano to carry out the experimental tests, specially on the acquisition of images to perform the digital image correlation study.

References

[1] R. A. McMaster, Flat Glass Tempering - How It Works, Glass Industry (1989) 10–15.

[2] A. K. Varshneya, Chemical Strengthening of Glass: Lessons Learned and Yet To Be Learned, International Journal of Applied Glass Science 1 (2010) 131–142. arXiv:arXiv:1011.1669v3, doi:10.1111/j.2041-1294.2010.00010.x.

[3] S. Karlsson, B. Jonson, C. Stålhandske, The technology of chemical glass strengthening - A review, Glass Technology: European Journal of Glass Science and Technology Part A 51 (2) (2010) 41–54. doi:10.1128/MCB.23.4.1181-1195.2003.

[4] A. Berenjian, G. Whittleston, History and manufacturing of glass Title History and manufacturing of glass History and Manufacturing of Glass, American Journal of Materials Science (1) (2017) 18–24. doi:10.5923/j.materials.20170701.03.

[5] R. Hess, Material Glass, Structural Engineering International: Journal of the International Association for Bridge and Structural Engineering (IABSE) 14 (2) (2004) 76–79.

[6] K. C. Datsiou, M. Overend, The strength of aged glass, Glass Structures & Engineering 2 (2) (2017) 105–120. doi:10.1007/s40940-017-0045-6.

[7] R. Gy, Ion exchange for glass strengthening, Materials Science and Engineering B: Solid-State Materials for Advanced Technology 149 (2) (2008) 159–165. doi:10.1016/j.mseb.2007.11.029.

[8] R. Gardon, Thermal Tempering of Glass, in: D. Uhlmann, N. Kreidl (Eds.), Glass Science and Technology, Academic Press, Inc., 1980, pp. 145–216. doi:10.1016/B978-0-12-706705-6.50010-2.

[9] P. J. Lezzi, R. O. Maschmeyer, J. C. Thomas, K. L. Wasson, Thermally tempered glass and methods and apparatuses for thermal tempering of glass (2016).

[10] F. Monnoyer, D. Lochegnies, Heat transfer and flow characteristics of the cooling system of an industrial glass tempering unit, Applied Thermal Engineering 28 (17-18) (2008) 2167–2177. doi:10.1016/j.applthermaleng.2007.12.014.

[11] Y. Chen, D. Lochegnies, R. Defontaine, J. Anton, H. Aben, R. Langlais, Measuring the 2D residual surface stress mapping in tempered glass under the cooling jets: The influence of process parameters on the stress homogeneity and isotropy, Strain 49 (1) (2013) 60–67. doi:10.1111/str.12013.

[12] J. H. Nielsen, J. F. Olesen, H. Stang, Characterization of the Residual Stress State in Commercially Fully Toughened Glass, Journal of Materials in Civil Engineering 22 (2) (2010) 179–185. doi:10.1061/(asce)0899-1561(2010)22:2(179).

[13] J. Anton, A. Errapart, M. Paemurru, D. Lochegnies, S. Hödemann, H. Aben, On the inhomogeneity of residual stresses in tempered glass panels, Estonian Journal of Engineering 18 (1) (2012) 3. doi:10.3176/eng.2012.1.01.

[14] CEN, prEN 13474-1. Glass in building – Design of glass panes – Part 1: General basis of design, 1999.

[15] D. I. f. B. (DIBt), TRAV - Technische Regeln für die Verwendung von absturzsichernden Verglasungen., 2003.

[16] M. Haldimann, Fracture strength of structural glass elements - analytical and numerical modelling , testing and design, Ph.D. thesis, École Polytechnique Fédérale de Lausanne (2006).

[17] M. Feldmann, R. Kaspar, B. Abeln, A. Gessler, K. Langosch, J. Beyer, J. Schneider, S. Schula, G. Siebert, A. Haese, F. Wellershoff, P. Cruz, J. Belis, J. Colvin, T. Morgan, F. Ensslen, M. Eliasova, Z. Šulcová, G. Royer-Carfagni, L. Galuppi, C. Grenier, H. Hoegner, R. Kruijs, C. Louter, G. Manara, J. Neugebauer, V. Rajcic, R. Zarnic, Guidance for European Structural Design of Glass Components, Tech. rep., Luxembourg (2014). doi:10.2788/5523.

[18] S. W. Freiman, Fracture Mechanics of Glass, in: D. Uhlmann, N. Kreidl (Eds.), Glass Science and Technology, Vol. 5, Academic Press, Inc., 1980, pp. 21–78. doi:10.1016/B978-0-12-706705-6.50007-2.

[19] S. Mohammadi, Extended Finite Element Analyasis, Blackwell Publishing Ltd, 2008. doi:10.1002/9780470697795.

[20] I. Llavori, J. A. Esnaola, A. Zabala, M. Larrañaga, X. Gomez, Fretting: Review on the Numerical Simulation and Modeling of Wear, Fatigue and Fracture, Contact and Fracture Mechanics (2017). doi:http://dx.doi.org/10.5772/46845.

[21] S. Chen, M. Zang, D. Wang, S. Yoshimura, T. Yamada, Numerical analysis of impact failure of automotive laminated glass: A review, Composites Part B: Engineering 122 (2017) 47–60. doi:10.1016/j.compositesb.2017.04.007.

[22] W. Gao, R. Wang, S. Chen, M. Zang, An intrinsic cohesive zone approach for impact failure of windshield laminated glass subjected to a pedestrian headform, International Journal of Impact Engineering 126 (October 2018) (2019) 147–159. doi:10.1016/j.ijimpeng.2018.12.013.

[23] D. Pietras, T. Sadowski, L. Wójcik, Impact of Exploitation Flaws on Load Capacity of Tempered Glass Stairs Assessed by Numerical Analysis with XFEM, in: 7th International Conference on Advanced Materials and Structures - AMS 2018, Vol. 416, 2018. doi:10.1088/1757-899X/416/1/012085.

[24] B. Egboiyi, R. Mattey, S. Konica, P. Nikam, S. Ghosh, T. Sain, Mechanistic understanding of the fracture toughening in chemically strengthened glass—experiments and phase-field fracture modeling, International Journal of Solids and Structures 238 (111374) (2022). doi:10.1016/j.ijsolstr.2021.111374.

[25] M. Overend, G. A. R. Parke, D. Buhagiar, Predicting Failure in Glass—A General Crack Growth Model, Journal of Structural Engineering 133 (8) (2007). doi:10.1061/(ASCE)0733-9445(2007)133:8(1146).

[26] F. A. Veer, P. C. Louter, F. P. Bos, The strength of annealed, heat-strengthened and fully tempered float glass, Fatigue and Fracture of Engineering Materials and Structures 32 (1) (2009) 18–25. doi:10.1111/j.1460-2695.2008.01308.x.

[27] Y. M. Rodichev, F. A. Veer, O. B. Soroka, O. A. Shabetya, Structural Strength of Heat-Strengthened Glass, Strength of Materials 50 (4) (2018) 584–596. doi:10.1007/s11223-018-0004-8.

[28] A. Ramos, M. Muniz-Calvente, P. Fernández, A. Fernández-Canteli, M. J. Lamela, Análisis probabilístico de elementos de vidrio recocido mediante una distribución triparamétrica Weibull, Boletin de la Sociedad Espanola de Ceramica y Vidrio 54 (4) (2015) 153–158. doi:10.1016/j.bsecv.2015.06.002.

[29] G. Pisano, G. R. Carfagni, Statistical interference of material strength and surface prestress in heat-treated glass, Journal of the American Ceramic Society 100 (3) (2017) 954–967. doi:10.1111/jace.14608.

[30] S. Schula, J. Schneider, M. Vandebroek, J. Belis, Fracture strength of glass, engineering testing methods and estimation of characteristic values, in: COST Action TU0905, Mid-term Conference on Structural Glass, Porec, Croatia, 2013, pp. 223–234.

[31] G. Castori, E. Speranzini, Fracture strength prediction of float glass: The Coaxial Double Ring test method, Construction and Building Materials 225 (2019) 1064–1076. doi:10.1016/j.conbuildmat.2019.07.264.

[32] M. Muniz-Calvente, A. Ramos, P. Fernández, M. J. Lamela, A. Álvarez, A. Fernández-Canteli, Probabilistic failure analysis for real glass components under general loading conditions, Fatigue and Fracture of Engineering Materials and Structures 42 (6) (2019) 1283–1291. doi:10.1111/ffe.13011.

[33] A. Bonati, A. Occhiuzzi, G. Pisano, G. Royer-Carfagni, A micro-mechanically motivated model for the strength of heat-treated glass, Glass Structures and Engineering 3 (2) (2018) 153–166. doi:10.1007/s40940-018-0071-z.

[34] M. Muniz-Calvente, A. M. de Jesus, J. A. Correia, A. Fernández-Canteli, A methodology for probabilistic prediction of fatigue crack initiation taking into account the scale effect, Engineering Fracture Mechanics 185 (2017) 101–113. doi:10.1016/j.engfracmech.2017.04.014.

[35] M. Muñiz-Calvente, A. Ramos, V. Shlyannikov, M. J. Lamela, A. Fernández-Canteli, Hazard maps and global probability as a way to transfer standard fracture results to reliable design of real components, Engineering Failure Analysis 69 (2016) 135–146. doi:10.1016/j.engfailanal.2016.02.004.

[36] J. H. Nielsen, K. Thiele, J. Schneider, M. J. Meyland, Compressive zone depth of thermally tempered glass, Construction and Building Materials 310 (125238) (2021). doi:10.1016/j.conbuildmat.2021.125238.

[37] European Standard, EN 1288-5: Glass in building - Determination of the bending strength of glass. Part 5: Coaxial double ring test on flat specimens with small test surface areas, Brussels, 2000.

[38] European Standard, EN 1288-1: Glass in building - Determination of the bending strength of glass. Part 1: Fundamentals of testing glass, Brussels, 2000.

[39] A. Iglesias, M. Martinez-Agirre, I. Torca, I. Llavori, J. A. Esnaola, Numerical methodology based on fluid-structure interaction to predict the residual stress distribution in glass tempering considering non-uniform cooling, Computers and Structures 264 (2022) 106757. doi:10.1016/j.compstruc.2022.106757.

[40] O. S. Narayanaswamy, Model of Structural Relaxation in Glass, Journal of the American Ceramic Society 54 (10) (1971) 491–498. doi:10.1111/j.1151-2916.1971.tb12186.x.

[41] J. H. Nielsen, J. F. Olesen, P. N. Poulsen, H. Stang, Finite element implementation of a glass tempering model in three dimensions, Computers and Structures 88 (17-18) (2010) 963–972. doi:10.1016/j.compstruc.2010.05.004.

[42] A. Ramos, Modelo probabilístico para el dimensionamiento de elementos de vidrio estructural bajo solicitación estática y dinámica, Ph.D. thesis, Universidad de Oviedo (2017).

[43] M. Mahmoud, Frictional Behavior of Different Glove Materials Sliding Against Glass Sheet, Journal of Applied Sciences 16 (10) (2016) 491–495. doi:10.3923/jas.2016.491.495.

[44] M. F. Ashby, H. Shercliff, D. Cebon, Friction and wear, in: Materials: engineering, science, processing and design, fourth edi Edition, Butterworth-Heinemann, 2019.

[45] R. Barnett, C. Connors, P. Hermann, J. Wingfield, Fracture of brittle materials under transient mechanical and thermal loading, Tech. rep.

(1967). doi:AFFDL-TR-66-220.

[46] A. Freudenthal, Statistical approach to brittle fracture, Academic Press, 1968.

[47] M. Muniz-Calvente, A. Ramos, F. Pelayo, M. J. Lamela, A. Fernández-Canteli, Statistical joint evaluation of fracture results from distinct experimental programs: An application to annealed glass, Theoretical and Applied Fracture Mechanics 85 (2016) 149–157. doi:10.1016/j.tafmec.2016.08.009.

[48] A. Bernard, E. C. Bos-Levenbach, The Plotting of Observations on Probability-paper, Statistica neerlandica 7 (3) (1953) 163–173. doi:https://doi.org/10.1111/j.1467-9574.1953.tb00821.x.

[49] MathWorks, Fitting a Univariate Distribution Using Cumulative Probabilities.
URL https://es.mathworks.com/help/stats/fitting-a-univariate-distribution-using-cumulative-probabilities.html;jsessionid=f62d01d571c710e689f33193f34c